A forward genetic screen in zebrafish identifies the G-protein coupled receptor CaSR as a modulator of sensorimotor decision-making

Roshan A. Jain[1,2,*], **Marc A. Wolman**[1,3], **Kurt C. Marsden**[1,4], **Jessica C. Nelson**[1], **Hannah Shoenhard**[1], **Fabio A. Echeverry**[6], **Christina Szi**[2], **Hannah Bell**[1,5], **Julianne Skinner**[1], **Emilia N. Cobbs**[2], **Keisuke Sawada**[2], **Amy Zamora**[2], **Alberto E. Pereda**[6], and **Michael Granato**[1,7,*]

[1]Department of Cell and Developmental Biology; University of Pennsylvania, Perelman School of Medicine; Philadelphia, PA, 19104; USA

[2]Department of Biology; Haverford College; Haverford, PA, 19041; USA

[6]Dominick P. Purpura Department of Neuroscience, Albert Einstein College of Medicine, Rose F. Kennedy Center, 1410 Pelham Parkway South, Bronx, NY 10461, USA

Summary

Animals continuously integrate sensory information and select contextually appropriate responses. Here we show that zebrafish larvae select a behavioral response to acoustic stimuli from a pre-existing choice repertoire in a context-dependent manner. We demonstrate that this sensorimotor choice is modulated by stimulus quality and history, as well as by neuromodulatory systems, all hallmarks of more complex decision-making. Moreover, from a genetic screen coupled with whole genome sequencing, we identified eight mutants with deficits in this sensorimotor choice, including mutants of the vertebrate-specific G-protein coupled extracellular *calcium-sensing receptor (CaSR)* whose function in the nervous system is not well understood. We demonstrate that *CaSR* promotes sensorimotor decision-making acutely through $G\alpha_{i/o}$ and $G\alpha_{q/11}$ signaling, modulated by clathrin-mediated endocytosis. Combined, our results identify the first set of genes critical for behavioral choice modulation in a vertebrate, and reveal an unexpected critical role for *CaSR* in sensorimotor decision-making.

eTOC Blurb

Correspondence granatom@pennmedicine.upenn.edu; rjain1@haverford.edu.
[3]Current address, Department of Integrative Biology; University of Wisconsin; Madison, WI, 53706; USA
[4]Current address, Department of Biological Sciences; North Carolina State University; Raleigh, NC, 27607; USA
[5]Current address, University of Rochester Medical Center; University of Rochester; Rochester, NY, 14642; USA
[7]Lead Contact

Declaration of Interests
The authors declare no competing interests.

Using larval zebrafish Jain et al. establish and validate a simple sensorimotor decision-making paradigm. Using this paradigm they perform a forward genetic screen that identifies the first set of vertebrate sensorimotor decision-making genes including the Calcium-Sensing Receptor that acts as a bidirectional regulator of sensorimotor choice.
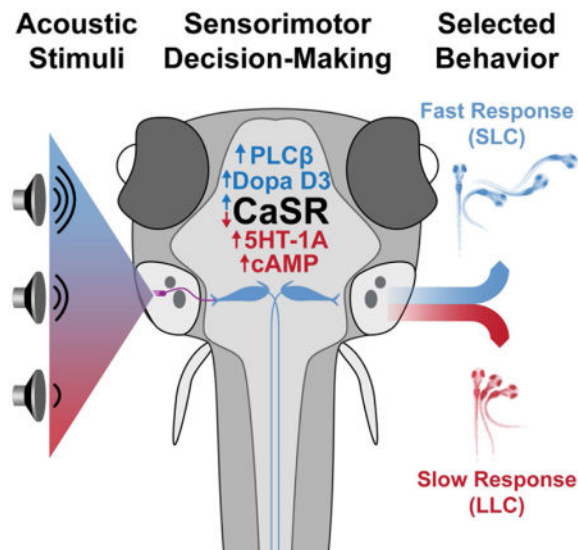
Keywords

Zebrafish; genetic screen; decision-making; behavior choice; startle response; Calcium-sensing receptor; CaSR; AP2S1

Introduction

Animals navigating their environment are challenged to prioritize one behavior over another. For example, terrestrial and aquatic vertebrates exposed to an abrupt acoustic stimulus can reorient to explore the stimulus source or perform a protective startle response to shield their body or escape a potential predator [1, 2]. The decision to perform one behavior over another depends not only on qualities relating to the stimulus, but also on prior experiences and context [3, 4]. Sources of context include the external environment such as the presence of predators or food, and internal states such as hunger, anxiety, or ongoing behaviors [5]. Across the wide range of decision-making complexity, each decision-making scenario ultimately represents behavioral selection and bias [6].

While decision-making can involve complex cognitive computation, simple behavioral choices in invertebrates and non-mammalian vertebrates are also dynamically modulated, providing the opportunity to use genetically tractable systems to study distinct steps of the decision-making process [7–11]. For example, *C. elegans* movement directionality is controlled by forward and backward motor circuits, and the interface between these circuits has been used to study decision-making for directional locomotion [12]. Similarly, optogenetic dissection of mechanosensory responses of *Drosophila* larvae has revealed different inhibitory circuit modules controlling behavioral selection, switching, and

maintenance in this simple context [13]. Finally, zebrafish larvae use visually guided decision-making to move toward or away from looming stimuli based on size, allowing pursuit of small prey and avoidance of large potential predators [14]. However, the molecular-genetic mechanisms underlying vertebrate decision-making, even for simple behavioral choices in larval zebrafish, are not well understood.

To establish a robust decision-making paradigm amenable to genetic screens, we used an evolutionarily conserved and ethologically relevant behavior, the acoustic startle response [15]. In response to acoustic stimuli zebrafish larvae execute one of two distinct motor behaviors: a Short-Latency C-bend (SLC) initiating within 5–15 milliseconds of the stimulus, or a slower, Long-Latency C-bend (LLC) response initiating within 20–80 milliseconds, (Figure 1A, Movie S1) [16]. Time projection analysis previously revealed that unlike the SLC response, LLC behavior usually does not displace the animal from its original location during a 40 ms time window typical of fast aquatic predator strikes, suggesting that selecting LLC maneuvers would be less effective to evade high speed attacks (Figure 1A). SLC and LLC responses are also readily distinguishable based on other kinematic parameters including angular velocity and turning angle [16]. One hallmark of decision-making is that distinct neural circuits mediate the different behavioral outcomes. Both SLC and LLC behaviors can be elicited by acoustic/vibrational stimuli, which zebrafish larvae detect through sensory hair cells of the lateral line (transmitted through the anterior and posterior lateral line ganglia) and the otic vesicle (transmitted via the VIIIth statoacoustic nerve), all of which project to the hindbrain, where they synapse on the lateral dendrite of the Mauthner cell and on other hindbrain neurons [17–19]. Mauthner ablation abolishes SLC responses without affecting LLC behavior, while loss of otoliths in the ear abolishes LLC but not SLC responses [16, 20]. Moreover, ablation of hindbrain spiral fiber neurons decreases SLC responses in favor of LLC responses [20]. Finally, pectoral fins remain adducted during SLCs while they are active during LLCs (Figure 1B and Movie S2) [21]. Thus, while the circuits underlying LLC versus SLC choice have not been fully mapped, SLCs and LLCs are not tunable variations of the same motor pattern but utilize different, possibly overlapping circuitry to generate distinct behaviors.

Here we establish and validate a robust and high-throughput behavioral paradigm using larval zebrafish to measure and quantify acoustically driven SLC versus LLC sensorimotor decision-making. Using this paradigm, we performed a forward-genetic screen and identified the first set of sensorimotor decision-making mutants in a vertebrate, including mutants of the extracellular *calcium-sensing receptor* (*CaSR*). Finally, we demonstrate a previously unknown regulatory role for the extracellular calcium sensing receptor *CaSR* in acutely modulating behavior, and identify key downstream effectors and regulators of CaSR signaling modulating sensorimotor decision-making *in viv*o.

Results

SLC versus LLC bias fulfills key criteria defining decision-making

To determine whether SLC versus LLC behavioral selection indeed reflects a simple decision behavior, we characterized additional criteria common to many well-established decision-making paradigms [8, 22]. First, we examined whether SLC versus LLC selection

simply reflects a fixed bias or whether it is influenced by stimulus quality. We thus examined response bias to a range of acoustic stimulus intensities where overall responsiveness increased as stimulus intensity increased, consistent with previous observations (Figure 1C) [16]. At weak stimulus intensities (4.6 dB) larvae were strongly biased to select LLC responses, which shifted to relatively unbiased selection at moderate intensities (13.5 dB) and strong SLC selection bias at high intensities (25.9 dB; Figure 1C). Thus, with increasing stimulus intensity larvae robustly shift their response bias from LLC to SLC behaviors.

We next tested whether larvae dynamically shift their acoustic response behavior based on prior experience [23]. For this we exposed larvae to a series of intense stimuli (25.9 dB) at 20 second intervals, followed by a series of 30 equally intense stimuli now spaced 1 second apart (Figure 1D). Although overall stimulus responsiveness eventually declined due to habituation [24], responding larvae rapidly shifted their relative bias from SLCs to LLCs during stimuli 11–20 when responsiveness was still >50% (Figure 1D). Importantly, this dynamic bias shift was not unique to 5 days postfertilization (dpf) larvae, as 29 dpf fish exposed to a similar paradigm of repeating stimuli also shifted their bias away from SLCs and towards LLCs (Figure S1), demonstrating that dynamic regulation of acoustic behavior selection in the mature nervous system is already functional in 5 dpf larvae.

Lastly, we tested whether neuromodulation characteristic of more complex decision-making also modulates SLC versus LLC choice. We screened a library of 1280 bioactive molecules with known targets for their acute effects on SLC versus LLC bias. From this screen we identified 95 compounds shifting bias from SLC to LLC following strong stimuli, and 54 compounds shifting bias from LLC to SLC following weak stimuli. We focused on a molecular subset predicted to modulate neurotransmission, including glutamatergic, cholinergic, purinergic, GABAergic as well as serotonergic and dopaminergic neurotransmission, observing a significant over-representation of compounds modulating serotonergic neurotransmission among those shifting bias toward LLC responses (Figure S2, Table S1). We confirmed that acute exposure to 5-HT1A receptor agonists (PAPP, S15535, and serotonin) effectively shifted bias from SLC to LLC following intense stimuli (Figures 1E, S2). Conversely, dopaminergic modulators were the largest class of drugs shifting bias toward SLC behavior, and acute exposure to a D3 agonist (7OHD) shifted bias from LLC to SLC following weak stimuli (Figure 1E), while exposure to a D3 antagonist shifted bias toward LLC behavior (Figure S2). Thus, acute pharmacological modulation of serotonergic and dopaminergic neurotransmission significantly and bidirectionally shift SLC versus LLC sensorimotor choice.

A forward genetic screen identifies zebrafish mutants with deficits in SLC versus LLC choice

To identify genes required for simple acoustic decision-making we performed a forward genetic screen in parallel to a previously reported screen for habituation mutants [25], screening third generation 5 dpf offspring from ENU-mutagenized males for their acoustic response bias. Larvae displaying any morphological phenotypes, hearing defects and/or a low (<40%) overall response rate to strong acoustic stimuli, or strong kinematic defects in the performance of SLC or LLC behaviors were excluded from further analyses. Through

this screen we identified eight mutants in which response bias to an intense stimulus was significantly shifted from SLC towards LLC responses. We quantified the extent to which SLC versus LLC bias was changed in each mutant (Figure 2A), revealing variations in the strength and/or penetrance of the bias shift phenotype between mutants, from nearly exclusive LLC-biased responses of *better late than never*[p193] and *late responder*[p196] to the milder effect of *procrastinator*[p192] (Figure 2A). Though most phenotypes were observed at frequencies suggesting recessive effects, the *biased*[dp197] allele produced a clear bias phenotype in half of the offspring of carrier outcrosses to wild type, indicating a dominant or haploinsufficient allele. All tested crosses between recessive carriers of different alleles showed phenotypic complementation, indicating that most or all of these mutations represent different genes (Table 1).

To test the behavioral specificity of our mutants, we measured overall acoustic responsiveness, spontaneous swimming activity, habituation learning, as well as visually-evoked turning behaviors (O-bends [26]). All mutants showed mild-to-no reductions in overall responsiveness to 26 dB stimuli, with *fashionably late*[p191] and *wrong turn*[p190] showing the largest and smallest reductions, respectively (Table 1). While such changes are not sufficient to account for the large response bias change, as many mutant individuals responded to 100% of stimuli with strong LLC biases, we cannot rule out additional mild impacts on acoustic sensitivity in some mutants. Spontaneous movement levels were indistinguishable from wild type for *wrong turn*[p190], *procrastinator*[p192], *better late than never*[p193], *snooze button*[p194], *indecisive*[p195], and *late responder*[p196] mutants, while *biased*[dp197] and *fashionably late*[p191] mutants displayed mildly increased and decreased levels of spontaneous movement, respectively (Table 1). No mutants displayed deficits in habituating to repeated acoustic stimuli (Table 1), highlighting that simple learning and decision-making processes are genetically separable. Similarly, responsiveness to visual (dark flash) stimuli was normal in all mutants. While *snooze button*[p194] and *better late than never*[p193] had shorter and longer visually-evoked response latencies respectively, the remaining mutants were indistinguishable from their siblings (Table 1), underscoring the overall specificity of the behavioral screen for acoustic sensorimotor decision-making.

To determine whether the identified mutants indeed affect sensorimotor decision-making, we focused on the *wrong turn* mutant because of its consistently strong phenotype (Figure 2B, Movie S3). While wild type larvae dynamically shift from LLC to SLC responses with increasing stimulus intensities, *wrong turn* mutants exhibited a strong bias towards LLC behaviors at all stimulus intensities (Figures 1C,2D). Moreover, *wrong turn* mutants display largely normal or mildly elevated overall responsiveness to acoustic stimuli despite their bias toward LLCs (Figure 2E), consistent with sensory acuity being largely unaffected in *wrong turn* mutants. We then tested whether prior experience would affect behavioral selection in these mutants, examining if they would shift their behavioral bias across repeated (1 sec ISI) identical acoustic stimuli. While wild type larvae rapidly shift their bias from SLC to LLC responses following repeated strong stimuli, *wrong turn* mutant fish maintain a bias toward LLC responses across repeated stimuli (Figure 2F). Though they don't shift bias, mutant larvae are still able to reduce their responsiveness through this experience at similar levels as their siblings, indicating their mechanisms for acoustic startle habituation remain intact (Table 1). To exclude the possibility that the *wrong turn* mutation simply increases startle

response latency, we compared the kinematic profiles of *wrong turn* short- and long-latency responses to those of sibling SLC and LLC behaviors. Overall, initial turn latencies, durations, maximal turning angles, and maximal angular velocities of the long-latency responses of *wrong turn* mutants resembled the parameters of sibling LLC responses and all were significantly distinct from sibling SLC responses (Figure S3). Similarly, short-latency responses of *wrong turn* mutants kinematically resembled sibling SLC responses, not LLC responses (Figure S3). Furthermore, *wrong turn* mutants used their pectoral fins extensively during long-latency responses and rarely during short-latency responses, just like their siblings (Figure 2C). Finally, to exclude that the *wrong turn* mutant phenotype is caused by delayed neural circuit development we examined 21 dpf juvenile *wrong turn* mutants, observing the same dramatic deficit in SLC versus LLC behavioral choice (Figure S3E–F). Combined, these results reveal a novel set of genetic mutations that selectively modulate SLC versus LLC behavioral choice, and identify the *wrong turn* gene to be critical for sensorimotor decision-making.

The G-protein coupled calcium sensing receptor (CaSR) regulates acoustic decision-making

The eight decision-making mutants isolated provide unique entry points to determine how sensorimotor decision-making in zebrafish is molecularly regulated. We focused on the *wrong turn* mutant to identify the causative molecular lesion via a whole-genome sequencing approach [25]. We first identified genomic regions of high homozygosity in a pool of behaviorally-selected *wrong turn* mutants, then verified linkage to a 800kb region of Chromosome 5 through bulked segregant analysis (Figure S4A) [25, 27]. Within this genomic region we identified a T-to-C nucleotide change that strongly segregated with the *wrong turn* phenotype and was absent in over 257 reads of related wild type control samples. This mutation changed amino acid 174 from a serine to proline in the coding sequence of the extracellular *Calcium Sensing Receptor* (*CaSR*) (Figure 2G). CaSR is a G-protein coupled receptor that detects alterations in extracellular calcium concentrations, best known for its critical role in modulating parathyroid hormone secretion and urinary calcium excretion [28]. Though expressed in the vertebrate CNS (Figure S5A), CaSR's function in the nervous system is not well understood [29–31].

The serine residue mutated in *wrong turn* is conserved across vertebrate *CaSR* orthologs (Figure 2G), and is a key residue in the hinge region of the extracellular domain critical for full CaSR activity [32], suggesting the mutation disrupts CaSR's calcium-sensing function. To confirm that mutations in *CaSR* cause the *wrong turn* behavioral phenotype, we generated a 7 bp deletion in *CaSR* causing a premature stop codon in the first transmembrane domain at position 613 of the *CaSR* protein (*CaSR^p198* Figures 2G, S4B). Trans-heterozygous larvae carrying both *wrong turn* and the new *CaSR^p198* allele exhibited the same behavior selection defect when exposed to intense stimuli, exhibiting a strong inappropriate bias towards LLC behaviors (Figure S4C). These data confirm that mutations in *CaSR* cause the *wrong turn* behavioral deficits, and identify *CaSR* as a critical regulator of sensorimotor decision-making.

In cultured neurons CaSR can regulate both neuronal morphology through neurite outgrowth [30], as well as neuronal activity and synaptic release [33, 34]. Given the striking decrease in SLC response selection by *CaSR* mutants, we first examined the morphology of the Mauthner command neuron, which is essential to elicit SLC behavior [16, 35–37]. Using a transgenic line expressing membrane-targeted citrine in Mauthner neurons, we measured the volume and surface area of the lateral and ventral dendrites receiving acoustic and visual inputs, respectively, as well as of the Initial Axon Segment (IAS) receiving input from spiral fiber neurons and the remaining Mauthner soma (Figure 3A–B) [25]. Volume and surface area of the axonal initial segment, and both ventral and lateral dendrites, were indistinguishable between *CaSR* mutants and wild type siblings (Figure 3C–D). However, *CaSR* mutants exhibited a mild increase in soma surface area without an increase in volume, suggesting a possible impact on Mauthner cell function (Figure 3C–D).

To test whether Mauthner neuronal function requires *CaSR*, we examined wild type and *CaSR* mutant Mauthner function through GCaMP6s calcium imaging and electrophysiological recordings. In wild type siblings short-latency startles were strongly associated with a robust calcium response in the Mauthner soma (Figure 3E,F,K) while minimal change was detected when long-latency startles were performed, consistent with published results (Figure 3G,K) [38]. *CaSR* mutant Mauthner soma showed a similar strong calcium response when short-latency startles were performed (Figure 3H,I,K). Similarly, when long-latency startles were performed, the calcium responses of *CaSR* mutant Mauthner soma were indistinguishable from those of their siblings (Figure 3J–K). We further investigated if changes in the excitability of the Mauthner neurons could explain or contribute to the behavioral phenotype of *CaSR* mutant fish through electrophysiological recordings. Whole-cell recordings revealed no alteration in rheobase (amount of current necessary to trigger an action potential), resting potential ($V_{resting}$), or input resistance (R_{in}) of *CaSR* mutant Mauthner neurons (Table S2). Though we observed a small increase in the Mauthner membrane potential threshold for action potential generation ($V_{Threshold}$, +4.6 mV in mutants), this difference alone does not represent a relevant modification of Mauthner neuron excitability and over 1/3 of mutant Mauthners had $V_{Threshold}$ within the range of wild type variation despite their strong behavioral phenotype.

We next explored if CaSR might be required for appropriate excitatory input to the Mauthner neuron, examining the role of the lateral line sensory organ, the distribution of electrical synapses important for Mauthner activation, and the level of excitatory calcium influx at the lateral dendrite. *CaSR* is expressed in the neuromasts of the lateral line sensory organ [39], so we reasoned that if *CaSR* regulates response selection here then disrupting the lateral line sensory input should impair larval decision-making. After ablating the sensory hair cells of the lateral line with neomycin, we observed no significant change in behavioral selection at any stimulus intensity tested (4.6–25.9 dB), indicating that CaSR is unlikely to impact behavioral selection at the level of sensory input from the lateral line organ (Figure S5F). Next we examined the distribution of Connexin 35/36 on the Mauthner cell surface to see if developmental assembly or maintenance of the major excitatory synaptic connections to the Mauthner require *CaSR*. In wild type animals, Connexin 35/36 immunoreactivity is enriched at large club ending synapses that transmit acoustically-evoked excitatory inputs to the lateral dendrite of the Mauthner neurons from the VIIIth statoacoustic nerve, as well as

at electrical synapses between spiral fiber neurons which provide excitatory input to the Mauthner initial axonal segment [40]. We observed no significant difference in the levels, localization, or number of Connexin 35/36 puncta in *CaSR* mutants compared to wild type siblings (Figure S5). Finally, we monitored GCaMP6s fluorescence in the Mauthner lateral dendrite in response to weak subthreshold acoustic stimuli to determine if excitatory calcium influx was altered in the dendrite. *CaSR* mutant and sibling larvae both showed similar dendritic activity to weak stimulation, arguing against a role for CaSR in Mauthner dendritic excitation (Figure S5G). Thus, while Mauthner neurons in *CaSR* mutants exhibit a mild increase in soma surface area and $V_{Threshold}$, the structure of major excitatory synaptic inputs as well as Mauthner activity during SLC and LLC responses are indistinguishable from those in wild type siblings, providing compelling evidence that instead of mediating SLC responses CaSR regulates the behavioral choice between SLC and LLC.

CaSR acutely regulates acoustic decision-making

We next tested whether CaSR regulates sensorimotor decision-making during development e.g. by establishing neural circuitry, or acutely e.g. by modulating neural activity. For this we first treated wild type individuals with two well characterized CaSR antagonists (Calhex-231 or NPS2143 [41]), from 24 hpf through 124 hpf, then tested their acoustic response bias. Whereas control DMSO-treated larvae exhibited a strong bias toward SLC responses to intense (26 dB) stimuli, Calhex-231 or NPS2143 treated larvae displayed dose-dependent changes in response bias to favor LLC responses, similar to *CaSR* mutant larvae (Figure 4A). We then restricted the period of CaSR antagonist treatment to distinguish between CaSR's roles in circuit development or function. Exposing larvae to CaSR antagonists during the period of circuit development (between 24–112 hpf) did not alter acoustic response bias (Figure 4B). In contrast, exposing larvae to CaSR antagonists only after the main period of circuit development (between 120–144 hpf) fully recapitulated the behavioral bias deficits observed in CaSR mutants (Figure 4B). Conversely, acutely exposing larvae to the CaSR agonist calindol for 30 minutes [42] significantly shifted larval behavioral bias toward SLC responses to low intensity stimuli (Figure 4C). While these CaSR modulators were also capable of affecting total larval responsiveness, under conditions with little-to-no responsiveness change we still observe clear significant shifts to acoustic response bias (Figure S6A–C). Thus, CaSR activity acutely and bidirectionally regulates acoustic decision-making.

CaSR functions as a canonical GPCR to regulate decision-making

CaSR has been shown to act by signaling through several G-proteins including $G\alpha_{i/o}$, $G\alpha_s$, and $G\alpha_{q/11}$ depending on the cell type, environment, and developmental status of the tissue (Figure 5A) [43]. CaSR activity can be regulated through clathrin-mediated endocytosis, which removes CaSR from the cell surface, thereby terminating its activity [44]. Given that CaSR signaling has been predominantly examined in non-neuronal tissues, we wondered whether CaSR regulates sensorimotor decision-making through $G\alpha_{i/o}$, $G\alpha_s$, or $G\alpha_{q/11}$, and/or whether clathrin-dependent pathways modulate CaSR's function in neurons. CaSR activity can regulate intracellular cAMP levels through $G\alpha_s$-dependent activation of adenylyl cyclase (AC) increasing cAMP, or through $G\alpha_{i/o}$-dependent inhibition of AC, reducing cAMP [43, 45, 46]. To test if either pathway modulates acoustic decision-making

in vivo, we pharmacologically increased cAMP levels in wild type larvae and examined whether this shifted their behavioral bias. For this we tested behavioral bias of larvae exposed to intense acoustic stimuli in the presence of 2.5 μM forskolin to activate AC. While control larvae displayed a strong bias toward SLC responses, forskolin-dependent AC activation shifted response bias toward LLC performances (Figure 5B). Moreover, exposing larvae to the phosphodiesterase IV (PDE4) inhibitor rolipram to inhibit cAMP degradation also shifted larval response bias toward LLC performance (Figure 5B). While rolipram can also impact responsiveness to acoustic stimuli at these levels, forskolin has minimal impact on responsiveness under conditions where behavioral selection is strongly altered (Figure S6D–E). If forskolin were shifting behavioral selection through an alternate signaling pathway, we might expect it to exacerbate the bias of *CaSR* mutants, however this level of forskolin does not significantly impact the *CaSR* bias phenotype (Figure 5B). In sum, acutely elevating cAMP levels recapitulates CaSR deactivation (Figure 4B), consistent with the idea that CaSR modulates acoustic decision-making - at least in part - via $G\alpha_{i/o}$ (Figure 5A).

CaSR also can signal through $G\alpha_q$ to activate Phospholipase C β (PLCβ), which generates DAG and IP_3 to increase intracellular Ca^{2+} [47, 48]. To test if this signaling pathway modulates acoustic decision-making, we exposed larvae to PLCβ inhibitor U73122 for 20 minutes, then determined behavioral bias. While DMSO-treated larvae were strongly biased toward SLC responses, U73122 treatment produced an acute dose-dependent shift in response bias toward LLCs (Figure 5C), phenocopying CaSR deactivation. Similar to other CaSR signaling modulators, U73122 can also impact overall larval responsiveness to acoustic stimuli, though a strong shift in behavioral bias is observed even at low concentrations with minimal responsiveness alteration (0.25 μM U73122), arguing that the decision-making phenotype is a direct effect of the drug rather than a secondary consequence (Figure S6F–G). Finally, we acutely exposed wild type larvae to PKC inhibitor PMA, which impairs CaSR/$G\alpha_{q/11}$ signaling-dependent intracellular Ca^{2+} increase in cell culture [49]. Acute exposure to 2.5 μM PMA shifted the bias of larvae toward LLC responses, supporting a role for PKC-dependent modulation of bias (Figure 5D), and further supporting the idea that CaSR signaling via $G\alpha_q$ modulates acoustic decision-making.

Finally, we tested whether CaSR dependent decision-making is also regulated by clathrin-mediated endocytosis. Specifically, the Adaptor Protein 2 (AP2) complex facilitates CaSR internalization from the plasma membrane by clathrin-mediated endocytosis, and mutations in both *CaSR* and the AP2 complex σ subunit (*AP2S1*) cause human hypercalcemia [50–52]. To determine whether the AP2 complex plays a role in CaSR dependent decision-making, we first examined acoustic startle bias in *ap2s1* mutants we isolated in a companion screen for startle modulation (Figure 6A, S7) [25]. We found that *ap2s1* mutants showed a strong bias toward SLC responses regardless of stimulus intensity (Figure 6B). Combined with the functional interaction between CaSR and AP2σ in cell culture [51], this suggested that *ap2s1* regulates sensorimotor decision-making by removing CaSR from the cell surface and hence terminating CaSR activity. This model predicts that partially reducing *ap2s1* and CaSR function simultaneously should ameliorate the LLC-shifted bias observed in *CaSR* mutants. Indeed, in response to strong (25.9 dB) stimuli when *CaSR* mutants inappropriately selected LLC behaviors, *CaSR; ap2s1* double mutants showed significant rescue of their bias

back toward SLC behavior (Figure 6C). Combined these data support the model that *CaSR* promotes sensorimotor decision-making acutely through $G\alpha_{i/o}$ and $G\alpha_{q/11}$ signaling, and that CaSR signaling is likely modulated via clathrin-mediated endocytosis.

Discussion

Selecting the most appropriate response from a pre-existing behavioral repertoire is crucial for individuals to successfully navigate their environment. Here we show that zebrafish larvae prioritize behavioral responses to acoustic stimuli with several key behavioral and pharmacological characteristics of dynamic decision-making in other animals [22, 23]. Through a forward genetic screen we identified a first set of genes underlying sensorimotor decision-making, including the vertebrate-specific G-protein coupled receptor *CaSR. CaSR* function is required to modulate response bias based on stimulus quality and history, two hallmarks of sensorimotor decision-making. Rather than regulating the execution of SLC or LLC behaviors, *CaSR* acts acutely in the selection process that enables larvae to prioritize SLC over LLC responses.

Zebrafish larvae exhibit robust sensorimotor decision-making

Using a combination of behavioral and pharmacological experiments we find that zebrafish larvae prioritize behavioral responses to acoustic stimuli with several key hallmarks of dynamic decision-making [22, 23]. First, at 5 dpf zebrafish larvae already possess the ability to select between the kinematically and neuronally distinct SLC and LLC behaviors evoked by the same stimuli. Response speed is critical for predator evasion in zebrafish and other small fish [53, 54] and unlike SLCs, LLCs produce minimal body displacement within 40 ms of acoustic stimuli, perhaps more consistent with a re-orientation behavior to evaluate non-threatening stimuli (Figure 1B). Thus LLC behavior is poorly suited for escape from likely fast-striking aquatic predators [55], and selection of the appropriate acoustic response is likely an ethologically relevant decision [56]. Second, the response selection mechanism is driven by stimulus quality, as larvae predictably shift their response bias from LLC to SLC behavior with increasing stimulus intensity, rather than using stochastic or fixed reflexive behavior selection mechanisms. Third, response selection is modulated and informed by prior experience. Though the acoustic responses examined here initiate on the order of a 4–80 ms, we demonstrate that behavioral response selection is carefully modulated and informed by experience accumulated over the course of several seconds (Figure 1D) [24]. Multiple modalities are integrated in the impact of this prior experience, as repeated inconsequential acoustic stimuli shift bias toward LLC behavior (Figure 1D), while exposure to tactile stimuli or visual stimuli can enhance subsequent SLC selection [24, 57]. Finally, acoustic behavior selection is modulated by serotonin and dopamine, conserved modulators of decision-making and behavioral bias from invertebrates to humans [58, 59]. Thus, LLC versus SLC response bias represents a quantifiable and high-throughput behavioral choice paradigm sharing key characteristics of more complex decision-making.

The role of CaSR in controlling behavioral bias

Using the observer independent and high-throughput behavioral paradigm outlined above, we conducted the first genetic screen for genes critical for vertebrate decision-making. We

demonstrate that the mutants we identified from this screen are all still capable of performing both SLC and LLC behaviors, so rather than merely disrupting performance of particular motor patterns, they instead reveal the genetic blueprint underlying the behavioral selection process itself (Figure 2A). Whole genome sequencing revealed an unexpected yet key role for *CaSR* in sensorimotor decision-making. CaSR has been extensively studied for its role in regulating parathyroid hormone secretion and serum calcium levels, with inactivating and activating *CaSR* mutations causing hypercalcemia or hypocalcemia in humans, respectively [28]. Defects of the nervous system and behavior have also been observed in humans with *CaSR* disruptions, including mental retardation, dementia, and epilepsy [60–62]. However, the extent to which these neural deficits are due to direct neuronal functions of CaSR or secondary effects of hormonal secretion or serum ion composition changes has been unclear. The Ser-174 residue mutated in *CaSR^{p190}* corresponds to the Ser-170 residue of human CaSR, and when mutated in cultured cells this strongly decreases CaSR signaling activity [32, 63]. CaSR crystal structures indicate this residue is located in a ligand binding pocket for extracellular aromatic amino acids and/or Ca^{2+} ions critical for CaSR activity and signaling [64, 65]. Thus, combined with the behavioral phenocopy produced by CaSR antagonists, the *CaSR^{p190}* mutation likely disrupts its ability to monitor and respond to a variety of extracellular molecular signals to modulate decision-making behavior.

CaSR mutant mice show both direct and indirect (hormonal) defects in brain development, neural proliferation, and neuronal morphology in culture [30, 66]. Treating zebrafish larvae with pharmacological CaSR modulators revealed a direct and acute role for CaSR in modulating sensorimotor decision-making (Figure 4). Moreover, acutely increasing or decreasing CaSR activity shifted behavioral bias in opposing directions, suggesting that rather than regulating a single circuit component/connection in an on/off manner, *CaSR* modulates the behavioral balance between SLC and LLC at several levels, for example by acting presynaptic and/or postsynaptically. Indeed, CaSR protein localizes to synapses [67], and presynaptic CaSR activation reduces glutamate release in cultured neurons through regulation of presynaptic cation channels [33]. Postsynaptically, CaSR activity modulates K + channel activity and nonselective cation channels to regulate their excitability [34, 68]. Paradoxically, CaSR can also enhance spontaneous release of both GABA and glutamate, which might support homeostatic plasticity and/or synaptic facilitation [34, 68–70]. Finally, CaSR also forms functional heterodimers with neurotransmitter receptors including GABA-B type, mGluR1, and mGluR5 receptors in neurons [71, 72], thus CaSR might also modulate responses to these associated neurotransmitters in sensorimotor decision-making circuits.

How then does CaSR regulate SLC versus LLC behavioral bias? Our data and previously published work support a model where acoustic stimuli can activate competing hindbrain escape circuits that drive SLC or LLC behavior [16, 73, 74]. Modulation by high CaSR activity, dopaminergic signaling through D3, and PLCβ activity would promote SLC circuit activity, while low CaSR activity, serotonergic signaling through 5HT1A, and increased adenylyl cyclase activity would instead favor activation of the LLC-driving circuitry (Figure 6D). Given the mutant and pharmacological phenotypes observed, normal CaSR activity is predicted to relieve inhibition onto the Mauthner neuron, while also enhancing excitatory drive on the Mauthner neurons, and/or dampening excitation of LLC command-like neurons.

To regulate Mauthner inhibition CaSR could act in feedforward PHP neurons to reduce glycine release at synapses on the Mauthner, or at the synapse between the VIIIth statoacoustic nerve and feedforward PHP neurons, presynaptically reducing glutamate release or postsynaptically hyperpolarizing the PHP neurons [17, 75, 76]. Disrupting CaSR function would thus increase PHP activity, over-silencing the Mauthner neurons and permitting the LLC circuit to dominate. CaSR could enhance Mauthner excitation by depressing inhibitory neurotransmission onto the spiral fiber neurons that receive indirect input from the auditory nerve and enhance Mauthner activity, as ablation of spiral fiber neurons produces a shift in SLC/LLC bias similar to *CaSR* mutants [20]. Though we observed mild increases in Mauthner surface area and $V_{Threshold}$, these did not impact Mauthner input resistance or excitability, and given the acute (30 minute) impact of pharmacological CaSR activation on behavior selection, neuronal morphology change is unlikely to be the primary role for CaSR in this process. Finally, CaSR could also act at the excitatory synapse on the predicted LLC command neurons to limit the excitation or response of these neurons, thus CaSR disruption would increase the activity of these neurons to promote LLC's. However, for this to be the primary site of CaSR action would also require a mechanism where Mauthner activity is inhibited by an activated LLC circuit, which is unlikely given the extremely short latency from stimulus to Mauthner activation. *CaSR* is expressed broadly throughout the zebrafish brain [29], thus determining the neuronal cell population in which *CaSR* is required for SLC versus LLC choice will narrow down the potential mechanisms of how *CaSR* modulates the acoustic decision-making process and reveal the neurons critical for this behavioral selection.

Circuit control of sensorimotor decision-making

Similar to zebrafish, *Drosophila* exhibit two related escape responses, a "short mode" jump response with short latency driven by descending Giant Fiber neurons or a more controlled "long mode" response with a longer latency involving coordinated wing movements and finer directional control driven through Giant Fiber-independent descending circuits [77]. The Giant Fiber circuit has a higher activation threshold than the parallel "long mode" circuit and can override "long mode" behavior to force a short takeoff. Thus, the relative timing of Giant Fiber versus non-Giant Fiber activation drives escape behavior selection. It is tempting to speculate that a similar mechanism biases SLC versus LLC behavior selection in zebrafish. Indeed, similar to the Giant Fiber-driven escape in *Drosophila*, zebrafish SLC behavior is an "all-or-nothing" response with stereotyped kinematic parameters regardless of stimulus quality, while LLC speed, angle, and latency are informed by the intensity of the stimulus to allow greater directional control [16]. Furthermore, goldfish Mauthner firing activates and silences arrays of hindbrain reticulospinal neurons [78]. Given the differences in latency, Mauthner activity might actively prevent and preempt activation of the LLC circuit (Figure 6D). For example, Mauthner neurons and MiD3cm reticulospinal neurons display complementary activity patterns that correlate with short- and long-latency responses to water pulses [73], making MiD3cm neurons candidate neurons for controlling acoustically-evoked LLC behavior. Goldfish MiD3cm neurons show a 10-fold lower activation threshold than Mauthners and fire with longer latency than Mauthners in response to strong VIIIth statoacoustic nerve activation [18], consistent with the relative timing mechanism underlying *Drosophila* escape selection. Future experiments using whole brain

imaging techniques in zebrafish are required to identify both the neurons driving LLC behavior and those impacting SLC versus LLC selection, and it will be of great interest to determine the degree of conservation in the sensorimotor decision-making mechanisms underlying ethologically relevant escape behaviors.

STAR Methods

CONTACT FOR REAGENT AND RESOURCE SHARING

Further information and requests for resources and reagents should be directed to and will be fulfilled by the Lead Contact, Michael Granato (granatom@pennmedicine.upenn.edu).

EXPERIMENTAL MODEL AND SUBJECT DETAILS

All experiments with zebrafish (*Danio rerio*) were approved by the University of Pennsylvania IACUC and/or the Haverford College IACUC. Wild type Tüpfel Long-fin (TLF) and Wik-L11 (Wik) strains were used for all experiments [25, 79]. Embryos and larvae were raised at 29°C on a 14-h:10-h light:dark cycle in E3 media as previously described [25]. ENU mutagenesis was performed on TLF and Wik wild type adult males using the protocol previously described [25, 80, 81]. The germline mutagenesis rate was measured by crossing mutagenized males to *albino*[b4]; *golden*[b1]; *sparse*[b5] triple mutant females [80]. *Tg(hsp70:GAL4FFDMC)130a* and *Tg(hsp70:GFF62A)* were provided by Koichi Kawakami [82, 83]. *Tg(UAS:gap43-citrine)* fish were provided by Jonathan Raper [84]. *Tg(UAS:gcamp6s)* fish were previously described [38]. Sex is not determined in zebrafish until 25–60 dpf so behavioral analyses of larvae and juvenile fish were performed without consideration of sex.

To generate mutant alleles through CRISPR/Cas9 in this study, targeting sgRNA were designed using ChopChop v2 [85], cloned by direct annealing and ligation of oligos into pDR274 (Table S3) [86], synthesized using T7 MEGAshortscript kit (Ambion), and purified by MEGAclear kit (Ambion). Commercial Cas9 protein (PNA Bio) was combined with each sgRNA and injected into 1-cell stage wild type TLF embryos (G0) to mutate the targeted genomic loci, and these mosaic G0 individuals were raised to adulthood and outcrossed to establish heterozygous carrier lines.

METHOD DETAILS

Behavioral recording—Larval and juvenile behavioral testing was performed as previously described [24, 25, 27], recorded from above at 1000fps or 500fps with either a Motionpro camera (Redlake) or a Fastec TS4 camera (Fastec Imaging). Larvae were held in individual 9×9mm wells of a laser-cut clear acrylic 4×4 testing arena mounted in a 6 cm petri lid, resting on a metal ring attached to a vibration exciter (4810; Brüel and Kjaer, Norcross, GA) [27]. Constant infrared illumination below the testing arena was provided by a 96-bulb infrared LED array (IR100; YYtrade) with a white plexiglass sheet above it for even diffuse illumination, and a white light LED bulb (PAR38 LED light; LEDlight.com) obliquely lit the arena from above. Acoustic vibrational stimuli (2ms duration, 1000 Hz waveforms) were delivered vertically by the vibrational exciter. Visual "dark flash" stimuli were delivered by abruptly turning off the overhead white LED for 1 second, while the entire

testing apparatus was shielded from ambient light by an opaque black vinyl enclosure. Acoustic and visual stimuli were controlled by a digital–analog card (PCI-6221; National Instruments, Austin, TX) using the DAQtimer program [26]. All acoustic stimuli were calibrated with a PCB Piezotronics accelerometer (#355B04) and signal conditioner (#482A21), and voltage outputs were converted to dB using the formula $dB = 20 \log(V/0.775)$. When measuring bias and responsiveness of larvae relative to varied stimulus intensities, the same larvae were exposed to all intensities of stimuli at 20 second interstimulus intervals to prevent habituation, with intensities interleaved, 10 total stimuli per each intensity level. Temporal projections in Figure 1A were recorded at 1000 fps combining frames every 5 ms. Temporal projections in Figure 2B were recorded at 500 fps combining frames every 4 ms.

Genetic screen and mapping—ENU-mutagenized adult males from the TLF and WIK strains were crossed with wild type females of the same strain, then inbred for three generations so that F3 offspring could be both screened for behavioral defects and used for molecular genetic mapping against F1 grandparents [25, 80, 81]. We screened 405 F2 families, with an estimated 614 mutagenized genomes screened. We measured the germline mutagenesis rate to be 0.09% by scoring crosses to *albino*[b4]; *golden*[b1]; *sparse*[b5] triple mutants [80]. For each F3 clutch, we tested 32 larvae at 5 dpf for their acoustic response bias to 10 high intensity (25.9 dB) stimuli presented at 20 sec ISI. We screened for clutches where at least 15–25% of larvae showed a significantly divergent acoustic response bias from wild type controls (typically individuals with acoustic startle biases <−40), indicating a recessive homozygous mutation affecting simple decision-making. We validated F2 carriers by confirming similar frequencies of behaviorally mutant offspring in 2 or more independent crosses, and we collected behaviorally mutant and sibling F3 individuals from each family for genetic mapping and sequencing. Any larvae displaying striking morphological phenotypes, strong kinematic defects in the stereotyped performance of SLC or LLC behaviors, hearing defects, and/or low (<40%) overall response rates to strong stimuli were excluded from analysis. We further confirmed that each putative mutant was heritable by outcrossing the isolated F2 carriers of each family to wild type TLF or WIK fish, then re-isolating new F3 adult carrier pairs that again produced clutches with the same decision-making defect in at least 15–25% of their (F4) offspring. Whole genome sequencing was performed on gDNA from a pool of 50 behaviorally-selected *wrong turn* or *ignorance is bliss* F3 larvae, sequenced with 100 bp paired-end sequencing on the Illumina HiSeq 2000 platform, and homozygosity analysis done using 463,379 SNP markers identified by sequencing gDNA from ENU-mutagenized TLF and WIK males as described previously [25]. In parallel, independent gDNA pools of 50 behaviorally-selected mutant and sibling F3 larvae were screened by PCR for linkage to a panel of 147 SSLP markers across the zebrafish genome through bulk segregant analysis [25, 27]. Candidate mutations were defined as those SNPs from the whole genome sequencing that were linked to the identified SSLP markers with <1% allele frequency in our reference sequence and >95% allele frequency in the mutant sample that altered the amino acid sequence (nonsense, missense, or splice site mutations). Complementation between mutant lines was assessed by crossing verified heterozygous carriers between mutants and analyzing 1–4 crosses with 48–64 offspring each for behavioral bias to 10 high intensity (25.9 dB) stimuli presented at 20 sec

ISI. Alleles were classified as complementing if <10% of each clutch showed a behavioral bias shift relative to wild type controls.

Pharmacology—The LOPAC-1280 library (Sigma) was used for the small molecule screen as previously described [24]. Wild type TLF fish in E3 embryo media were treated with 1:100 dilution of the stock concentration, typically producing a 10 μM final drug concentration in 1% DMSO. 8 wild type fish were tested per compound in the screen. For chronic treatment of fish with *CaSR* antagonists, sets of 25 embryos were treated in 8ml E3 plus 80μl drug in DMSO starting at 24 hpf. Bath E3 was exchanged daily with fresh E3 + drug. Experiments using R-(+)-7-Hydroxy-DPAT hydrobromide (7OHD, Sigma), PAPP (LY-165,163, Sigma), S15535 (Sigma), U-99194A maleate (Santa Cruz), calindol hydrochloride (Sigma), forskolin (Sigma), rolipram (Sigma), U73122 (Fisher), and phorbol 12-myristate 13-acetate (PMA, Sigma) were performed by treating wild type TLF larvae with indicated final concentrations of drug in E3 embryo media for 20 minutes prior to behavioral testing in the E3 medium still containing the drug (30 minutes for calindol). Experiments using Calhex-231 (Sigma) and NPS2143 hydrochloride (Sigma) were performed by treating embryos and/or larvae for the noted time periods. When treatment lasted longer than 1 day, fresh drug and E3 (or DMSO & E3 for controls) was replaced each day, and for 24–112 hpf treatments E3 containing drug was removed at 112 hpf and rinsed 3 times with fresh E3 + DMSO. For all drug experiments, the final DMSO concentration in E3 was 1% for drug-treated and control fish. For lateral line ablation, 40 μM neomycin (Sigma, N1142) was applied to 6 dpf larvae in E3 for 1 hour at 29°C. Larvae were washed 4× with E3 and given 3–4 hours recovery time at 29°C before behavioral testing. After testing, DASPEI (Invitrogen, D 426) staining of neuromasts was performed to confirm complete ablation, incubating larvae in 0.05% DASPEI in E3 for 15 min, followed by 2 E3 washes prior to imaging [87].

Mutant Genotyping—*CaSR^p190* fish were genotyped either using the KASP method with proprietary primer sequences (LGC Genomics), or by amplifying the genomic locus with primers designed through the dCAPS program [88] followed by digestion by HinfI (NEB) to specifically digest the mutant allele (Table S3). The *ap2s1^p172* allele was genotyped by amplifying with dCAPS-designed primers (Table S3) followed by digestion by BsmAI (NEB) to specifically digest the mutant allele. CRISPR-generated mutant alleles were identified by amplifying the targeted region (see Table S3) and testing for a loss of a restriction site (BsaJI for *CaSR^p198*, MscI for *ap2s1^p199*).

Immunofluorescent Imaging—Larvae were fixed for 4 hours at room temperature in Sweet Fix (4% paraformaldehyde, 4% sucrose, 1× PBS pH 7.4) then brains were manually exposed by peeling away skin and jaw parts surrounding the brain with fine forceps. Tissue was permeabilized for 45 minutes with 0.1% collagenase in PBS (Sigma C-9891), then blocked in incubation buffer (0.2% BSA, 2% normal goat serum, 0.5% Triton-X100, 1% DMSO in 1× PBS pH7.4) Antibodies were diluted in incubation buffer and then used to detect their antigens in the fixed, dissected brains using Rabbit anti-GFP (1:500, Life Technologies) and Mouse anti-Cx35/36 (1:200, Millipore) primary antibodies, and Alexa488 Goat anti-Rabbit and Alexa594 Goat anti-Mouse IgG, highly cross-adsorbed secondary

antibodies (1:500, Life Technologies). Brains were then mounted in vectashield (Vector Labs), saving the individual tails matching each brain for subsequent genotyping. Images were acquired using a Zeiss LSM-710 confocal microscope.

In situ hybridization—To generate a probe for *CaSR* mRNA, we first amplified wild type zebrafish *CaSR* cDNA containing the full coding sequence and a portion of the 3′ UTR from 120 hpf larval total RNA using *CaSR* cDNA cloning primers (Table S3) and directly cloned it into pCRII-TOPO (ThermoFisher). We linearized the plasmid with BamHI (NEB), and synthesized an antisense DIG-labeled RNA probe using T7 RNA polymerase (Promega). Larvae were raised in E3 with 0.003% phenylthiourea to minimize pigment development, then were fixed in 4% paraformaldehyde/PBS and stored in methanol at −20°C. Larvae were permeabilized with 0.1% collagenase in 1× PBS for 2 hours, washed with PBS+0.1% Tween-20, then prehybridized at 65°C in hybridization solution [50% formamide, 5×SSC buffer, 50 μg/ml heparin, 5 mg/ml torula yeast RNA, 0.1% Tween-20, pH 6.0 adjusted with citric acid], followed by overnight incubation in hybridization buffer with DIG-labeled probe RNA at 65°C. Larvae were washed at 65°C with 50% formamide/2×SSC/0.1% Tween-20, then 2×SSC/0.1% Tween-20, then 0.2×SSC/0.1% Tween-20, followed by room temperature washing in MABT [100 mM maleic acid, 150 mM NaCl, 0.1% Tween-20, pH 7.5], blocking in MABT supplemented with 2% BM Block reagent (Sigma), 5% Normal Goat Serum, 2 mg/ml BSA, then overnight incubation with anti-DIG-AP antibody (1:3000, Roche) in blocking solution at room temperature. Larvae were washed with MABT then TMNT [100 mM Tris pH 9.5, 50 mM $MgCl_2$, 100 mM NaCl, 0.1% Tween-20, 1mM levamisole], and probe was detected with BM Purple reagent (Sigma). Stained larvae were mounted in 70% glycerol and imaged with a SPOT Insight 2Mp camera.

Calcium Imaging—Mauthner calcium imaging and analysis was performed as previously detailed [38]. Larvae were semi-restrained in 2% low melting point agarose with tails freed distal to the swim bladder. GCaMP6s images were captured with a Leica DM16000 B inverted spinning disk confocal at 20 Hz and tail movements with a Dalsa Genie HM640 camera at 500 Hz. We stimulated head-restrained larvae with 13.1 dB (intense) or −15 dB (subthreshold) acoustic stimuli, separating stimuli by at least 3 minutes to avoid habituation.

Electrophysiology—Electrophysiological recordings were conducted on wild type and *CaSR*[p190] mutant 5–6 dpf zebrafish, blind to *CaSR* genotype. Each larva also expressed membrane-targeted citrine in the Mauthner neurons for visualization: *Tg(hsp70:GAL4FFDMC)130a; Tg(UAS:gap43-citrine)*. Larvae were paralyzed with d-tubocurarine (10 μM, Sigma) in external solution (in mM: 134 NaCl, 2.9 KCl, 2.1 $CaCl_2$, 1.2 $MgCl_2$, 10 HEPES, 10 Glucose, pH 7.8 adjusted with NaOH) then placed on their backs and held with pins in a Sylgard-coated small culture dish (FluoroDish, WPI). The brain was exposed ventrally following the procedure described by Koyama et al [89]. Next, the dish containing the larvae was placed in the recording setup and superfused with external solution throughout the recording session. The Mauthner were identified by far-red DIC optics and citrine fluorescence. The patch pipette (3–4 MΩ) was filled with internal solution (in mM: 105 K-Methanesulfonate, 10 HEPES, 0.1 EGTA, 2 $MgCl_2$, 4 Na_2ATP, 0.4 Tris-GTP, 10 K2-Phosphocreatine, 23 mannitol, pH 7.2 adjusted with KOH). The liquid junction potential was

estimated in −16 mV using Clampex 10.6 (Molecular Devices). Whole-cell recordings were performed under current-clamp configuration and the bridge balance adjusted. The rheobase, defined as the minimum amount of positive current required to elicit an action potential, was determined by delivering a 10 ms current pulse of increasing magnitude. The voltage threshold was defined as the membrane potential value at which the depolarizing-current step elicits an action potential. The input resistance was estimated using the voltage deflection caused by a hyperpolarizing-current step of −1 nA and 10 ms duration, followed by derivation of resistance with Ohm's law. Recordings were performed on a single Mauthner neuron per larva, and larval genotypes were determined for each individual tested after analysis was complete.

QUANTIFICATION AND STATISTICAL ANALYSIS

Statistical analysis was performed using Graphpad Prism 6 and Microsoft Excel 14.1. Box-and-whisker plots indicate the median with whiskers extending to minimum and maximum data points. Error bars on bar plots and dot plots always indicate SEM. Student's two-tailed t-test with Welch's correction for unequal variance was used in pair-wise comparisons unless otherwise stated, using the Bonferroni correction for multiple comparisons where appropriate. Fisher's Exact Test was used to look for over-representation of drug targets from the LOPAC-1280 library and pectoral fin usage with Prism. The Kruskal Wallis test was used to examine the impact of varying stimulus intensity on larval startle bias using Prism. Statistical significance was defined as $p<0.05$ in each statistical test, and the significance is shown within figures and/or in the figure legends.

Behavioral Analyses—5–7 dpf larval behavior was tracked and scored using Flote software [26], while juvenile fish behavior and all pectoral fin movement scoring was performed manually, blind to genotype. To test startle bias, fish were exposed to 10 identical acoustic stimuli at 20s Inter-Stimulus Intervals (ISI) Relative Startle Bias Index was calculated using the formula: $100\% \times$ (SLC frequency − LLC frequency)/(total SLC + LLC response frequency), producing a range from +100% (all SLC) to −100% (all LLC). To test acoustic habituation of decision-making mutants with a baseline inherent bias toward LLC behavior that performed few SLC responses, we calculated the habituation of the *total* acoustic response rate (SLC and LLC behaviors combined) using the formula: $100\% \times$ (% Total responses to stimuli 31–40 at 1s ISI)/(% Total baseline responses to stimuli 1–10 at 20s ISI). Unless otherwise specified, mutant data presented consists of individuals that were tested and scored blindly then molecularly genotyped (where mutations were known) after all testing was complete. For secondary behavioral characterization presented in Table 1, larvae were generated from adult carriers 1–4 generations subsequent to the F2 generation of the initial screen shown in Figure 2A. Relative Bias and Total Response % in Table 1 were calculated from the larvae with the lowest 25% Relative Bias in the clutch of carriers. The remaining behaviors of Table 1 were tested on behaviorally-selected individuals with Relative Bias (26 dB) of +100% for siblings and <−60% for mutants. Since *biased*[dp197] showed a clear dominant phenotype in heterozygotes, larval progeny of *biased*[dp197] heterozygous carriers crossed to wild type are presented in Table 1. All *CaSR* mutant data presented in Table 1 were from subsequently genotype-verified larvae. Spontaneous activity was calculated by measuring average distance traveled per second over 160 seconds.

LOPAC-1280 Chemical Screen—Larvae responding to <50% of strong stimuli (ISI 20 sec) were excluded from analysis, and compounds where treatment resulted in <3 analyzable individuals were also excluded. For each treatment, 3 Z-scores of the bias change relative to all other tested and analyzed sibling fish tested that day were calculated using the following formula: Z-score = (Treated Bias – Avg Bias of Experimental Day)/(Std Deviation of Bias for Experimental Day), with typically 450–600 analyzable fish per experimental day. Z_{weak} examined responses to 10 weak stimuli (5–10 dB at 20 sec ISI), Z_{strong} examined responses to 10 strong stimuli (25.9 dB at 20 sec ISI), and $Z_{habituation}$ was the average Z-score across 3 blocks of 10 habituating strong stimuli (25.9 dB, 1 sec ISI, 30 total stimuli).

Mauthner Structural Imaging—Confocal stacks were used to quantify Mauthner morphology with Imaris 8 software (Bitplane) by creating a Mauthner surface based on the anti-GFP immunofluorescent signal from *Tg(GFFDMC130A);Tg(UAS:gap43-citrine)* expression. The lateral dendrite (LD) was manually segmented from the Mauthner with a vertical plane at 30μm from the most lateral distal point along the axis of the Mauthner soma, which included all club ending synapses into the LD region in all samples. The ventral dendrite (VD) was manually segmented by creating a cut plane at the inflection point between the ventral dendrite and the soma. The remaining central portion was defined as the soma. Neighboring blood cells occasionally labeled in this transgenic line were manually masked as necessary to avoid distorting quantifications. Quantification of Cx35 was performed through Imaris by first using the Mauthner surface to mask the Cx35 signal to isolate signal within the Mauthner neuron, then measuring total Cx35 signal in each segmented region. We manually measured Cx35-labeled club endings by creating surfaces from the masked Cx35 channel and counting the number of surfaces on the LD that had volumes greater than 750 voxels. Segmenting, masking, and quantification were performed blind to genotype.

Calcium Imaging—Behavioral latency was determined by manually examining tail videos for the first frame of tail movement, and GCaMP6s fluorescence changes were analyzed using Image J (NIH). Identically sized ROIs were manually created for the Mauthner soma and background, and the mean pixel value of the background ROI was subtracted from the mean of each target ROI for all images in the sequence to calculate the intensity at each time point. F_0 was calculated by averaging the intensity of the 20 time points (1 s) immediately prior to the acoustic stimulus. We defined Mauthner firing as a fluorescence change $\Delta F/F$ >0.4 in the soma, above which 95% of contralateral short-latency (<10ms) responses fell for siblings and no instances of long-latency responses or non-responses exceeded this. Imaging and analysis was performed blind to genotype, and each larva was genotyped after completion of the analyses.

Supplementary Material

Refer to Web version on PubMed Central for supplementary material.

Acknowledgments

References

1. Eaton, RC., editor. Neural Mechanisms of Startle Behavior. Boston, MA: Springer US; 1984.

2. Sillar, KT., Picton, LD., Heitler, WJ. The Neuroethology of Predation and Escape. Chichester, UK: John Wiley & Sons, Ltd; 2016.

3. Lima SL, Dill LM. Behavioral decisions made under the risk of predation: a review and prospectus. Canadian journal of zoology. 1990; 68:619–640.

4. Sillar, KT., Picton, LD., Heitler, WJ. The Neuroethology of Predation and Escape. John Wiley & Sons; 2016.

5. Palmer CR, Kristan WB. Contextual modulation of behavioral choice. Current Opinion in Neurobiology. 2011; 21:520–526. [PubMed: 21624826]

6. Gold JI, Shadlen MN. The neural basis of decision making. Annu Rev Neurosci. 2007; 30:535–574. [PubMed: 17600525]

7. Korn H, Faber DS. The Mauthner Cell Half a Century Later: A Neurobiological Model for Decision-Making? Neuron. 2005; 47:13–28. [PubMed: 15996545]

8. Kristan WB. Neuronal decision-making circuits. Current Biology. 2008; 18:R928–32. [PubMed: 18957243]

9. Wolpert DM, Landy MS. Motor control is decision-making. Current Opinion in Neurobiology. 2012; 22:996–1003. [PubMed: 22647641]

10. Doya K, Shadlen MN. Decision making. Current Opinion in Neurobiology. 2012; 22:911–913. [PubMed: 23177659]

11. Glimcher, PW. Decisions, Uncertainty, and the Brain: the Science of Neuroeconomics. Cambridge, Mass: MIT Press; 2003.

12. Kawano T, Po MD, Gao S, Leung G, Ryu WS, Zhen M. An imbalancing act: gap junctions reduce the backward motor circuit activity to bias *C. elegans* for forward locomotion. Neuron. 2011; 72:572–586. [PubMed: 22099460]

13. Jovanic T, Schneider-Mizell CM, Shao M, Masson JB, Denisov G, Fetter RD, Mensh BD, Truman JW, Cardona A, Zlatic M. Competitive Disinhibition Mediates Behavioral Choice and Sequences in *Drosophila*. Cell. 2016; 167:858–870e19. [PubMed: 27720450]

14. Barker AJ, Baier H. Sensorimotor Decision Making in the Zebrafish Tectum. Curr Biol. 2015; 25:2804–2814. [PubMed: 26592341]

15. Korn H, Faber DS. Escape behavior - brainstem and spinal cord circuitry and function. Current Opinion in Neurobiology. 1996; 6:826–832. [PubMed: 9000017]

16. Burgess HA, Granato M. Sensorimotor gating in larval zebrafish. J Neurosci. 2007; 27:4984–4994. [PubMed: 17475807]

17. Hatta K, Korn H. Physiological properties of the Mauthner system in the adult zebrafish. J Comp Neurol. 1998; 395:493–509. [PubMed: 9619502]

18. Nakayama H, Oda Y. Common sensory inputs and differential excitability of segmentally homologous reticulospinal neurons in the hindbrain. J Neurosci. 2004; 24:3199–3209. [PubMed: 15056699]

19. Pujol-Martí J, López-Schier H. Developmental and architectural principles of the lateral-line neural map. Front Neural Circuits. 2013; 7:47. [PubMed: 23532704]

20. Lacoste AMB, Schoppik D, Robson DN, Haesemeyer M, Portugues R, Li JM, Randlett O, Wee CL, Engert F, Schier AF. A convergent and essential interneuron pathway for Mauthner-cell-mediated escapes. Curr Biol. 2015; 25:1526–1534. [PubMed: 25959971]

21. McClenahan P, Troup M, Scott EK. Fin-tail coordination during escape and predatory behavior in larval zebrafish. PLoS ONE. 2012; 7:e32295. [PubMed: 22359680]

22. Ernst M, Paulus MP. Neurobiology of decision making: a selective review from a neurocognitive and clinical perspective. Biological Psychiatry. 2005; 58:597–604. [PubMed: 16095567]

23. Pearson JM, Watson KK, Platt ML. Decision making: the neuroethological turn. Neuron. 2014; 82:950–965. [PubMed: 24908481]

24. Wolman MA, Jain RA, Liss L, Granato M. Chemical modulation of memory formation in larval zebrafish. PNAS. 2011; 108:15468–15473. [PubMed: 21876167]

25. Wolman MA, Jain RA, Marsden KC, Bell H, Skinner J, Hayer KE, Hogenesch JB, Granato M. A genome-wide screen identifies PAPP-AA-mediated IGFR signaling as a novel regulator of habituation learning. Neuron. 2015; 85:1200–1211. [PubMed: 25754827]

26. Burgess HA, Granato M. Modulation of locomotor activity in larval zebrafish during light adaptation. J Exp Biol. 2007; 210:2526–2539. [PubMed: 17601957]

27. Jain RA, Wolman MA, Schmidt LA, Burgess HA, Granato M. Molecular-genetic mapping of zebrafish mutants with variable phenotypic penetrance. PLoS ONE. 2011; 6:e26510. [PubMed: 22039502]

28. Tfelt-Hansen J, Brown EM. The calcium-sensing receptor in normal physiology and pathophysiology: a review. Critical Reviews in Clinical Laboratory Sciences. 2005; 42:35–70. [PubMed: 15697170]

29. Herberger AL, Loretz CA. Morpholino oligonucleotide knockdown of the extracellular calcium-sensing receptor impairs early skeletal development in zebrafish. Comparative Biochemistry and Physiology Part A: Molecular & Integrative Physiology. 2013; 166:470–481.

30. Vizard TN, O'Keeffe GW, Gutierrez H, Kos CH, Riccardi D, Davies AM. Regulation of axonal and dendritic growth by the extracellular calcium-sensing receptor. Nature Neuroscience. 2008; 11:285–291. [PubMed: 18223649]

31. Yano S, Brown EM, Chattopadhyay N. Calcium-sensing receptor in the brain. Cell Calcium. 2004; 35:257–264. [PubMed: 15200149]

32. Zhang Z, Qiu W, Quinn SJ, Conigrave AD, Brown EM, Bai M. Three adjacent serines in the extracellular domains of the CaR are required for L-amino acid-mediated potentiation of receptor function. J Biol Chem. 2002; 277:33727–33735. [PubMed: 12095982]

33. Phillips CG, Harnett MT, Chen W, Smith SM. Calcium-sensing receptor activation depresses synaptic transmission. J Neurosci. 2008; 28:12062–12070. [PubMed: 19005071]

34. Smith SM, Chen W, Vyleta NP, Williams C, Lee CH, Phillips C, Andresen MC. Calcium regulation of spontaneous and asynchronous neurotransmitter release. Cell Calcium. 2012; 52:226–233. [PubMed: 22748761]

35. Eaton RC, DiDomenico R, Nissanov J. Role of the Mauthner cell in sensorimotor integration by the brain stem escape network. Brain Behav Evol. 1991; 37:272–285. [PubMed: 1933251]

36. Kimmel CB, Hatta K, Metcalfe WK. Early axonal contacts during development of an identified dendrite in the brain of the zebrafish. Neuron. 1990; 4:535–545. [PubMed: 2322459]

37. Burgess HA, Johnson SL, Granato M. Unidirectional startle responses and disrupted left-right coordination of motor behaviors in *robo3* mutant zebrafish. Genes, Brain and Behavior. 2009; 8:500–511.

38. Marsden KC, Granato M. In Vivo Ca(2+) Imaging Reveals that Decreased Dendritic Excitability Drives Startle Habituation. Cell Reports. 2015; 13:1733–1740. [PubMed: 26655893]

39. Kwong RWM, Auprix D, Perry SF. Involvement of the calcium-sensing receptor in calcium homeostasis in larval zebrafish exposed to low environmental calcium. Am J Physiol Regul Integr Comp Physiol. 2014; 306:R211–21. [PubMed: 24381181]

40. Jabeen S, Thirumalai V. Distribution of the gap junction protein connexin 35 in the central nervous system of developing zebrafish larvae. Front Neural Circuits. 2013; 7:91. [PubMed: 23717264]

41. Petrel C, Kessler A, Dauban P, Dodd RH, Rognan D, Ruat M. Positive and negative allosteric modulators of the Ca2+-sensing receptor interact within overlapping but not identical binding sites in the transmembrane domain. J Biol Chem. 2004; 279:18990–18997. [PubMed: 14976203]

42. Kessler A, Faure H, Petrel C, Ruat M, Dauban P, Dodd RH. N2-benzyl-N1-(1-(1-naphthyl)ethyl)-3-phenylpropane-1,2-diamines and conformationally restrained indole analogues: development of calindol as a new calcimimetic acting at the calcium sensing receptor. Bioorg Med Chem Lett. 2004; 14:3345–3349. [PubMed: 15149704]

43. Conigrave AD, Ward DT. Calcium-sensing receptor (CaSR): pharmacological properties and signaling pathways. Best Practice & Research Clinical Endocrinology & Metabolism. 2013; 27:315–331. [PubMed: 23856262]

44. Ray K. Calcium-Sensing Receptor: Trafficking, Endocytosis, Recycling, and Importance of Interacting Proteins. Prog Mol Biol Transl Sci. 2015; 132:127–150. [PubMed: 26055057]

45. Chen CJ, Barnett JV, Congo DA, Brown EM. Divalent Cations Suppress 3′,5′-Adenosine Monophosphate Accumulation by Stimulating a Pertussis Toxin-Sensitive Guanine Nucleotide-Binding Protein in Cultured Bovine Parathyroid Cells. Endocrinology. 1989; 124:233–239. [PubMed: 2462488]

46. Mamillapalli R, VanHouten J, Zawalich W, Wysolmerski J. Switching of G-protein usage by the calcium-sensing receptor reverses its effect on parathyroid hormone-related protein secretion in normal versus malignant breast cells. J Biol Chem. 2008; 283:24435–24447. [PubMed: 18621740]

47. Ward DT. Calcium receptor-mediated intracellular signalling. Cell Calcium. 2004; 35:217–228. [PubMed: 15200145]

48. Rey O, Young SH, Jacamo R, Moyer MP, Rozengurt E. Extracellular calcium sensing receptor stimulation in human colonic epithelial cells induces intracellular calcium oscillations and proliferation inhibition. J Cell Physiol. 2010; 225:73–83. [PubMed: 20648625]

49. Bai M, Trivedi S, Lane CR, Yang Y, Quinn SJ, Brown EM. Protein kinase C phosphorylation of threonine at position 888 in Ca2+o-sensing receptor (CaR) inhibits coupling to Ca2+ store release. J Biol Chem. 1998; 273:21267–21275. [PubMed: 9694886]

50. Pollak MR, Brown EM, Chou YHW, Hebert SC, Marx SJ, Stelnmann B, Levi T, Seidman CE, Seidman JG. Mutations in the human Ca2+-sensing receptor gene cause familial hypocalciuric hypercalcemia and neonatal severe hyperparathyroidism. Cell. 1993; 75:1297–1303. [PubMed: 7916660]

51. Nesbit MA, Hannan FM, Howles SA, Reed AAC, Cranston T, Thakker CE, Gregory L, Rimmer AJ, Rust N, Graham U, et al. Mutations in *AP2S1* cause familial hypocalciuric hypercalcemia type 3. Nat Genet. 2013; 45:93–97. [PubMed: 23222959]

52. Breitwieser GE. The calcium sensing receptor life cycle: trafficking, cell surface expression, and degradation. Best Practice & Research Clinical Endocrinology & Metabolism. 2013; 27:303–313. [PubMed: 23856261]

53. Wainwright PC, Ferry-Graham LA, Waltzek TB, Carroll AM, Hulsey CD, Grubich JR. Evaluating the use of ram and suction during prey capture by cichlid fishes. J Exp Biol. 2001; 204:3039–3051. [PubMed: 11551992]

54. Walker JA, Ghalambor CK, Griset OL, McKenney D, Reznick DN. Do faster starts increase the probability of evading predators? Functional Ecology. 2005; 19:808–815.

55. Webb PW. Body and fin form and strike tactics of four teleost predators attacking fathead minnow (Pimephales promelas) prey. Canadian Journal of Fisheries and Aquatic Science. 1984; 41:157–165.

56. Herberholz J, Marquart GD. Decision Making and Behavioral Choice during Predator Avoidance. Front Neurosci. 2012; 6:125. [PubMed: 22973187]

57. Mu Y, Li XQ, Zhang B, Du JL. Visual input modulates audiomotor function via hypothalamic dopaminergic neurons through a cooperative mechanism. Neuron. 2012; 75:688–699. [PubMed: 22920259]

58. Rogers RD. The roles of dopamine and serotonin in decision making: evidence from pharmacological experiments in humans. Neuropsychopharmacology. 2011; 36:114–132. [PubMed: 20881944]

59. Mesce KA, Pierce-Shimomura JT. Shared strategies for behavioral switching: understanding how locomotor patterns are turned on and off. Front Behav Neurosci. 2010:4. [PubMed: 20179788]

60. Sfar S, Bzéouich AA, Kerkeni E, Bouaziz S, Najjar MF, Chouchane L, Monastiri K. A novel *CASR* mutation in a Tunisian FHH/NSHPT family associated with a mental retardation. Mol Biol Rep. 2012; 39:2395–2400. [PubMed: 21667241]

61. Conley YP, Mukherjee A, Kammerer C, DeKosky ST, Kamboh MI, Finegold DN, Ferrell RE. Evidence supporting a role for the calcium-sensing receptor in Alzheimer disease. Am J Med Genet B Neuropsychiatr Genet. 2009; 150B:703–709. [PubMed: 19035514]

62. Kapoor A, Satishchandra P, Ratnapriya R, Reddy R, Kadandale J, Shankar SK, Anand A. An idiopathic epilepsy syndrome linked to 3q13.3-q21 and missense mutations in the extracellular calcium sensing receptor gene. Ann Neurol. 2008; 64:158–167. [PubMed: 18756473]

63. Silve C, Petrel C, Leroy C, Bruel H, Mallet E, Rognan D, Ruat M. Delineating a Ca2+ binding pocket within the venus flytrap module of the human calcium-sensing receptor. J Biol Chem. 2005; 280:37917–37923. [PubMed: 16147994]

64. Geng Y, Mosyak L, Kurinov I, Zuo H, Sturchler E, Cheng TC, Subramanyam P, Brown AP, Brennan SC, Mun H-C, et al. Structural mechanism of ligand activation in human calcium-sensing receptor. Elife. 2016:5.

65. Zhang C, Zhang T, Zou J, Miller CL, Gorkhali R, Yang JY, Schilmiller A, Wang S, Huang K, Brown EM, et al. Structural basis for regulation of human calcium-sensing receptor by magnesium ions and an unexpected tryptophan derivative co-agonist. Sci Adv. 2016; 2:e1600241. [PubMed: 27386547]

66. Liu XL, Lu YS, Gao JY, Marshall C, Xiao M, Miao DS, Karaplis A, Goltzman D, Ding J. Calcium sensing receptor absence delays postnatal brain development via direct and indirect mechanisms. Mol Neurobiol. 2013; 48:590–600. [PubMed: 23564401]

67. Ruat M, Molliver ME, Snowman AM, Snyder SH. Calcium sensing receptor: molecular cloning in rat and localization to nerve terminals. PNAS. 1995; 92:3161–3165. [PubMed: 7724534]

68. Jones BL, Smith SM. Calcium-Sensing Receptor: A Key Target for Extracellular Calcium Signaling in Neurons. Front Physiol. 2016; 7:116. [PubMed: 27065884]

69. Kavalali ET. The mechanisms and functions of spontaneous neurotransmitter release. Nat Rev Neurosci. 2015; 16:5–16. [PubMed: 25524119]

70. Jin I, Puthanveettil S, Udo H, Karl K, Kandel ER, Hawkins RD. Spontaneous transmitter release is critical for the induction of long-term and intermediate-term facilitation in *Aplysia*. PNAS. 2012; 109:9131–9136. [PubMed: 22619320]

71. Chang W, Tu C, Cheng Z, Rodriguez L, Chen TH, Gassmann M, Bettler B, Margeta M, Jan LY, Shoback D. Complex formation with the Type B gamma-aminobutyric acid receptor affects the expression and signal transduction of the extracellular calcium-sensing receptor. Studies with HEK-293 cells and neurons. J Biol Chem. 2007; 282:25030–25040. [PubMed: 17591780]

72. Gama L, Wilt SG, Breitwieser GE. Heterodimerization of calcium sensing receptors with metabotropic glutamate receptors in neurons. J Biol Chem. 2001; 276:39053–39059. [PubMed: 11489900]

73. Kohashi T, Oda Y. Initiation of Mauthner- or non-Mauthner-mediated fast escape evoked by different modes of sensory input. J Neurosci. 2008; 28:10641–10653. [PubMed: 18923040]

74. Takahashi M, Inoue M, Tanimoto M, Kohashi T, Oda Y. Short-term desensitization of fast escape behavior associated with suppression of Mauthner cell activity in larval zebrafish. Neuroscience Research. 2017

75. Weiss SA, Preuss T, Faber DS. A role of electrical inhibition in sensorimotor integration. PNAS. 2008; 105:18047–18052. [PubMed: 19004764]

76. Koyama M, Minale F, Shum J, Nishimura N, Schaffer CB, Fetcho JR. A circuit motif in the zebrafish hindbrain for a two alternative behavioral choice to turn left or right. Elife. 2016:5.

77. von Reyn CR, Breads P, Peek MY, Zheng GZ, Williamson WR, Yee AL, Leonardo A, Card GM. A spike-timing mechanism for action selection. Nature Neuroscience. 2014; 17:962–970. [PubMed: 24908103]

78. Neki D, Nakayama H, Fujii T, Matsui-Furusho H, Oda Y. Functional motifs composed of morphologically homologous neurons repeated in the hindbrain segments. J Neurosci. 2014; 34:3291–3302. [PubMed: 24573288]

79. Rauch GJ, Granato M, Haffter P. A polymorphic zebrafish line for genetic mapping using SSLPs on high-percentage agarose gels. Technical Tips Online. 1997; 2:148–150.

80. Dosch R, Wagner DS, Mintzer KA, Runke G, Wiemelt AP, Mullins MC. Maternal control of vertebrate development before the midblastula transition: mutants from the zebrafish I. Developmental Cell. 2004; 6:771–780. [PubMed: 15177026]

81. Mullins MC, Hammerschmidt M, Haffter P, Nüsslein-Volhard C. Large-scale mutagenesis in the zebrafish: in search of genes controlling development in a vertebrate. Current Biology. 1994; 4:189–202. [PubMed: 7922324]

82. Pujol-Martí J, Zecca A, Baudoin JP, Faucherre A, Asakawa K, Kawakami K, López-Schier H. Neuronal birth order identifies a dimorphic sensorineural map. J Neurosci. 2012; 32:2976–2987. [PubMed: 22378871]

83. Yamanaka I, Miki M, Asakawa K, Kawakami K, Oda Y, Hirata H. Glycinergic transmission and postsynaptic activation of CaMKII are required for glycine receptor clustering in vivo. Genes Cells. 2013; 18:211–224. [PubMed: 23347046]

84. Lakhina V, Marcaccio CL, Shao X, Lush ME, Jain RA, Fujimoto E, Bonkowsky JL, Granato M, Raper JA. Netrin/DCC signaling guides olfactory sensory axons to their correct location in the olfactory bulb. J Neurosci. 2012; 32:4440–4456. [PubMed: 22457493]

85. Labun K, Montague TG, Gagnon JA, Thyme SB, Valen E. CHOPCHOP v2: a web tool for the next generation of CRISPR genome engineering. Nucleic Acids Res. 2016; 44:W272–6. [PubMed: 27185894]

86. Hwang WY, Fu Y, Reyon D, Maeder ML, Tsai SQ, Sander JD, Peterson RT, Yeh JRJ, Joung JK. Efficient genome editing in zebrafish using a CRISPR-Cas system. Nat Biotechnol. 2013; 31:227–229. [PubMed: 23360964]

87. Harris JA, Cheng AG, Cunningham LL, MacDonald G, Raible DW, Rubel EW. Neomycin-induced hair cell death and rapid regeneration in the lateral line of zebrafish (Danio rerio). J Assoc Res Otolaryngol. 2003; 4:219–234. [PubMed: 12943374]

88. Neff MM, Turk E, Kalishman M. Web-based primer design for single nucleotide polymorphism analysis. Trends in Genetics. 2002; 18:613–615. [PubMed: 12446140]

89. Koyama M, Kinkhabwala A, Satou C, Higashijima SI, Fetcho J. Mapping a sensory-motor network onto a structural and functional ground plan in the hindbrain. PNAS. 2011; 108:1170–1175. [PubMed: 21199937]

Highlights

- Zebrafish larvae exhibit robust acoustically-evoked decision-making

- Forward genetic screen identifies sensorimotor decision-making mutants

- Screen reveals a previously unknown role for the G-protein coupled receptor *CaSR*

- *CaSR* acutely regulates sensorimotor decision-making through $G\alpha_{i/o}$ & $G\alpha_q$ signaling
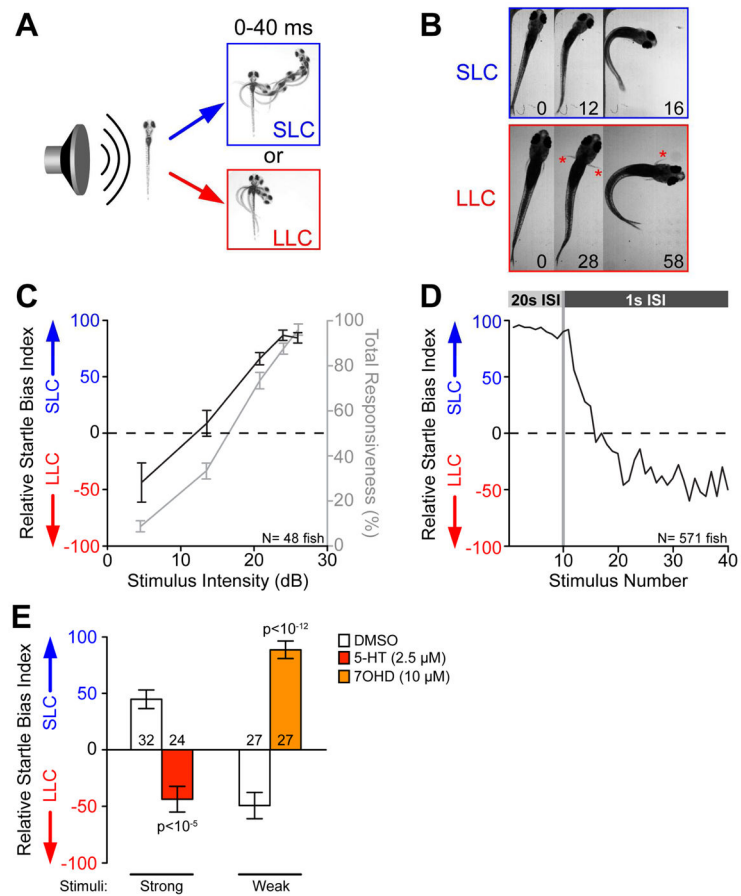
**Figure 1. Selection of appropriate behavioral responses to acoustic stimuli is a dynamic process**

(A) Temporal projections over 40 ms post-stimulus of wild type 5 dpf larvae performing SLC and LLC behaviors.

(B) Time course of the initial C-bend of wild type (WIK) fish performing SLC and LLC responses, 16 dpf. Numbers show elapsed time (ms) after stimulus, red asterisks indicate active pectoral fin usage. See also Movie S1.

(C) Average behavioral bias (black, left axis) and response frequency (grey, right axis) of 48 larvae (5 dpf) to acoustic stimuli (p<0.0001, Kruskal Wallis Test). Relative Startle Bias Index calculated for each larva at each intensity (see STAR Methods).

(D) Average relative startle bias of 5 dpf larvae following identical 26 dB stimuli at 20 sec intervals (Stimuli 1–10), then 1 sec intervals (stimuli 11–40). See also Figure S1.

(E) Average relative startle bias of 5 dpf larvae treated for 20 min with serotonin (5-HT) or dopamine D3 receptor agonist R-(+)-7-Hydroxy-DPAT (7OHD). Number of larvae tested at base of bars. Error bars indicate SEM. See also Figure S2, Table S1.
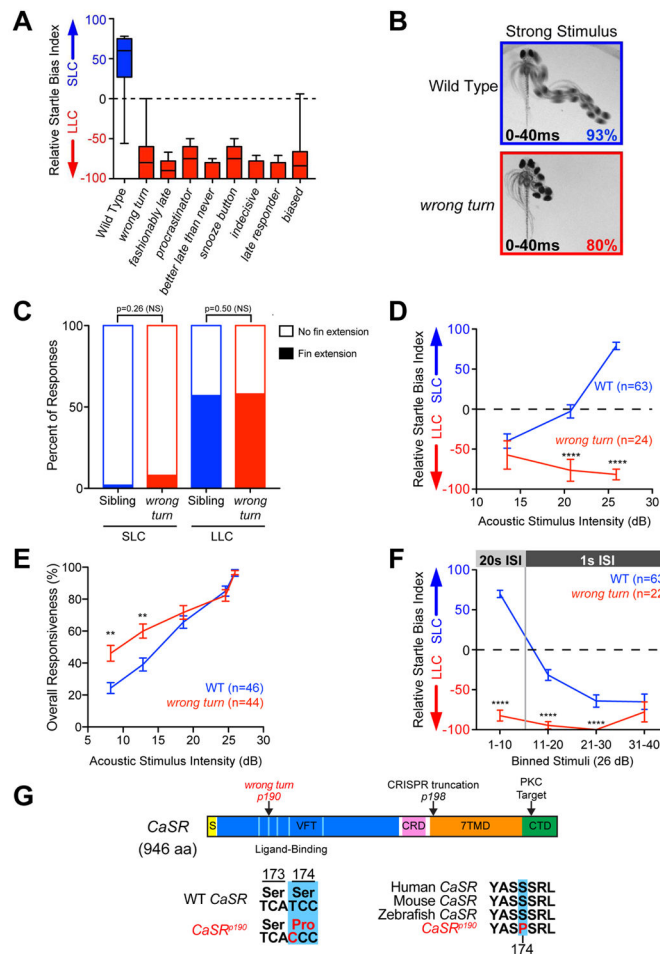
Figure 2. Isolation of decision-making mutants from a forward genetic screen

(A) Average startle biases of decision-making mutants, presenting average bias of the "bottom 25%" of all tested larvae from heterozygous mutant carrier incrosses (n 47 mutant larvae each), with the bottom 25% of representative wild type larvae (TLF, blue n=28).

(B) Temporal projection over 40 ms post-stimulus (26 dB) of wild type and *wrong turn* mutant 5 dpf larval responses. Percentage indicates average frequency observed (30 WT and 58 *wrong turn* larvae). See also Figure S3.

(C) Percent of short- and long-latency responses using pectoral fins during the initial C-bend. N=14 sibling (blue, 250 responses),14 *wrong turn* (red, 112 responses), Fishers Exact Test.

(D–E) Acoustic stimulus intensity vs average relative startle index (D) or average overall startle responsiveness (E) for wild type (blue) and *wrong turn* mutants (red).

(F) Average relative startle bias of 5 dpf *wrong turn* and wild type larvae following identical 26 dB stimuli at 20 sec intervals (Stimuli 1–10), then 1 sec intervals (stimuli 11–40).

(G) Zebrafish CaSR protein showing locations of *wrong turn*[p190] and *CaSR*[p198] mutations, Signal Sequence (S, yellow), extracellular Venus Fly Trap domain (VFT, blue), Cysteine-Rich Domain (CRD, pink), 7-pass transmembrane domain (7TMD, orange), C-Terminal Domain (CTD, green), 5 key residues of the ligand-binding pocket of the VFT hinge (light blue), and PKC phosphorylation residue (arrowhead). See also Figure S4.
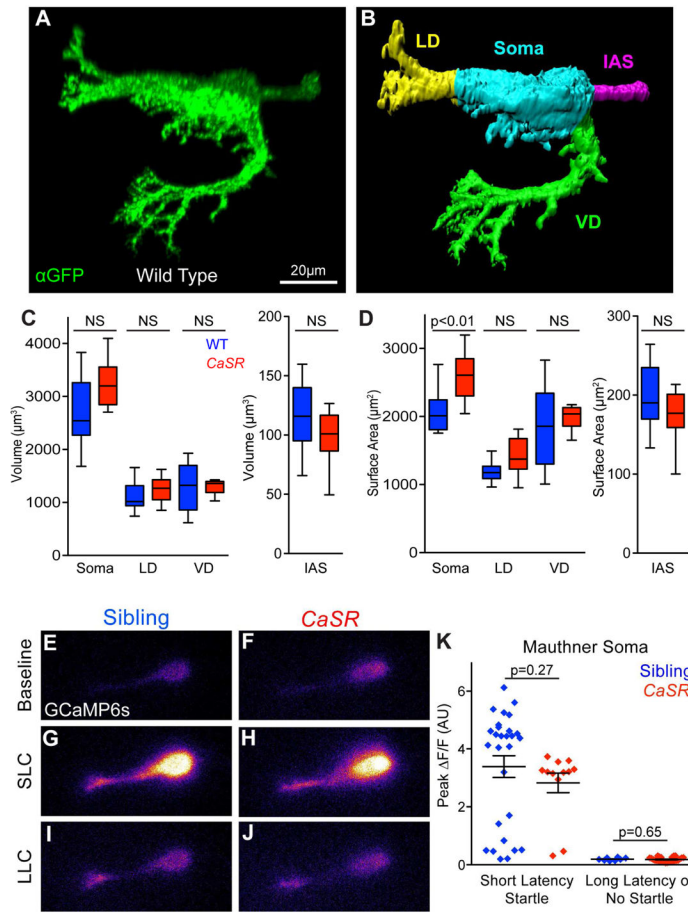
Error bars indicate SEM, **p<0.01, ****p<0.0001, Bonferroni-corrected t-test.

Figure 3. Mauthner morphology and function are largely unperturbed in *CaSR* mutants
(A) Representative projection of wild type Mauthner neuron expressing membrane-targeted gap43-citrine, stained with anti-GFP. Non-Mauthner labeling was thresholded and neurons reoriented for clarity.

(B) Surface of wild type Mauthner neuron from (A) segmented into the Lateral Dendrite (LD, yellow), Ventral Dendrite (VD, green), Initial Axon Segment (IAS, magenta), and Soma (cyan) for morphological quantification.

(C–D). Quantification of the volume (C) and surface area (D) of segmented Mauthner neuron regions (N=15 Sibling, 12 *CaSR* mutant neurons). See also Figure S5.

(E–J) Representative GCaMP6s fluorescence in Mauthner neurons of sibling (E, G, I) and *CaSR* mutant (F, H, J) larvae. Baseline fluorescence immediately prior to stimuli (E, F), and peak fluorescence during SLC (G, H) or LLC (I, J).

(K) Peak F/F in Mauthner soma during responses of sibling (blue) and *CaSR* mutant (red) larvae to 13 dB acoustic stimuli. N=28 Sibling SLC responses, 12 *CaSR* SLC responses, 8 Sibling LLC responses, 26 *CaSR* LLC responses. See also Table S2.
Error bars indicate SEM.
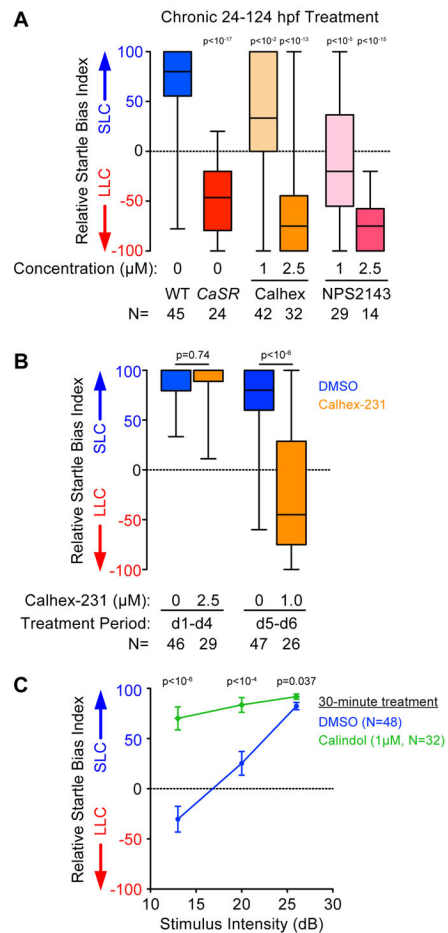
Figure 4. Pharmacological modulation of CaSR activity regulates acoustic decision-making
(A) Chronic treatment (24–124 hpf) with CaSR antagonists Calhex-231 and NPS2143 shifts average decision-making bias of wild type larvae toward LLC behavior.
(B) Relative startle bias of 6 dpf larvae following exposure to CaSR antagonist Calhex during circuit development (24–112 hpf) or post-circuit development (120–144 hpf).
(C) Decision-making bias of 5 dpf larvae following 30 minute acute activation of CaSR with 1μM Calindol. Error bars indicate SEM, Bonferroni-corrected t-test vs. DMSO control. See also Figure S6.
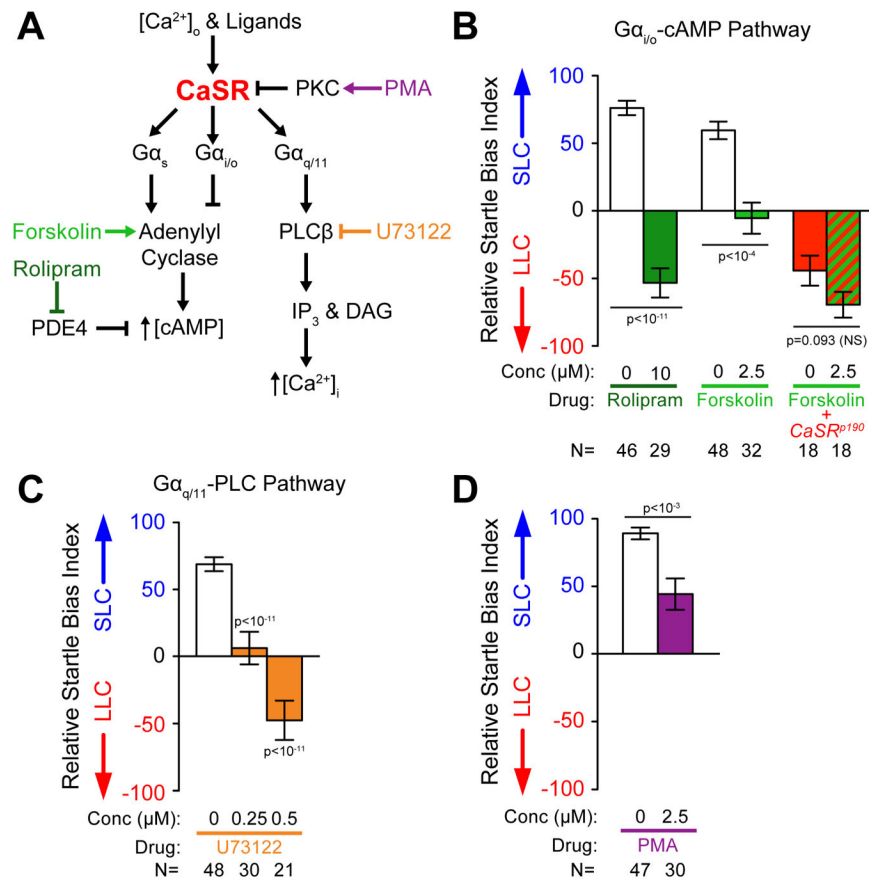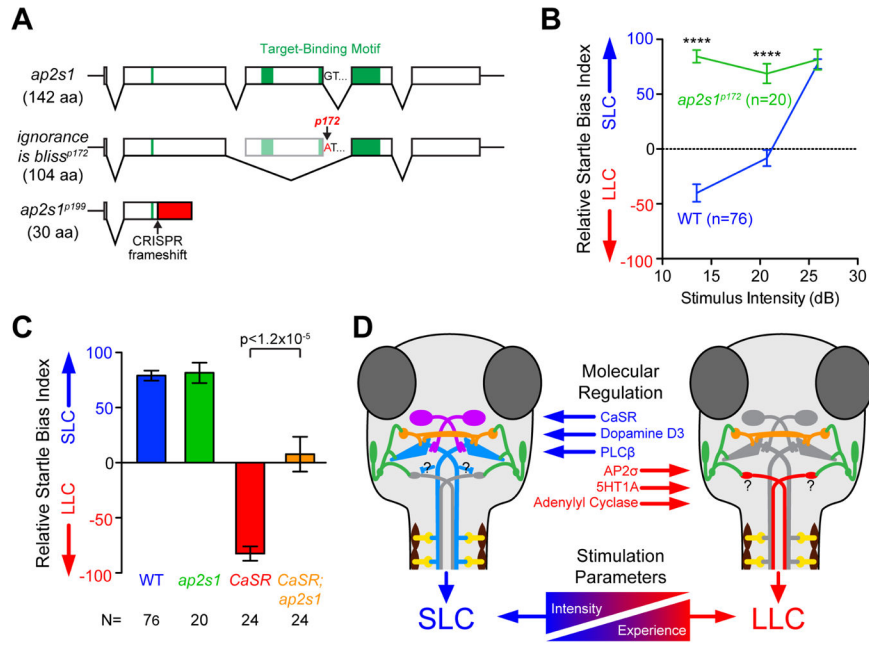
Figure 5. Molecular pathways of CaSR signaling and regulation control acoustic decision-making

(A) Molecular pathways implicated in CaSR signaling and regulation.

(B–D) Average startle bias index of 5 dpf larvae following 20 minute acute drug treatments. Disruption of $G\alpha_{i/o}$/cAMP signaling produced with 10μM rolipram or 2.5 μM forskolin **(B)**, disruption of $G\alpha_{q/11}$ signaling produced with U73122 **(C)**, and activation of PKC with phorbol 12-myristate 13-acetate (PMA) **(D)**.

Error bars indicate SEM, significance by Bonferroni-corrected t-test vs. DMSO control. See also Figure S6.

Figure 6. Molecular pathways of CaSR signaling and regulation control acoustic decision-making

(A) Diagram of *ap2s1* alleles and motifs. See also Figure S7.

(B) Average relative startle bias of *ap2s1^p172^* mutants.

(C) Average relative startle bias of 5 dpf wild type, *ap2s1^p172^*, *CaSR^p190^*, *CaSR^p190^;ap2s1^p172^* double mutant larvae, at 25.9 dB. ****p<0.0001

(D) General model of acoustic sensorimotor decision-making: Hair cells and VIIIth statoacoustic nerve (green), Mauthner neurons (blue), spiral fiber neurons (violet), feedforward PHP inhibitory neurons (orange), spinal motor neurons (yellow), proposed LLC command neurons (red).

Error bars indicate SEM, significance by t-test.

Table 1

Behavioral characterization of decision-making mutant larvae.

Mutant Allele	Relative Bias (26 dB)	Total Response % (26 dB)	Relative Bias (13 dB)	Spontaneous Activity (pixels/sec)	Acoustic Startle Habituation	Visual (Dark Flash) Response Latency (ms)	Complementing Alleles
wrong turn p190 (CaSR)	−75±4 (N=58)	93±1 (vs 98, p<10^{-2})	−57±18 (vs −41, p=0.54)	55±5 (vs 51, p<0.97)	68%±6 (vs 72%, p<0.66)	366±23 (vs 330, p=0.16)	*p191, p192, p196*
fashionably late p191	−72±3 (N=69)	77±3 (vs 96, p<10^{-7})	−83±10 (vs −58, p=0.09)	20±1 (vs 27, p<10^{-5})	56%±7 (vs 41%, p<0.06)	n.d.	*p190, p192, p193*
procrastinator p192	−30±4 (N=58)	84±4 (vs 94, p<10^{-3})	−97±3 (vs −46, p<0.0001)	30±1 (vs 27, p<0.10)	70%±5 (vs 72%, p<0.74)	198±7 (vs 188, p=0.29)	*p190, p191*
better late than never p193	−93±1 (N=65)	67±4 (vs 77, p<0.11)	−57±8 (vs −52, p=0.75)	37±1 (vs 39, p<0.26)	94%±2 (vs 94%, p<0.95)	270±7 (vs 246, p=0.019)	*p191*
snooze button p194	−40±4 (N=74)	83±3 (vs 96±1, p<10^{-4})	−33±18 (vs −36, p=0.90)	24±1 (vs 24, p<0.64)	92%±3 (vs 79%, p<0.0005)	244±23 (vs 327, p=0.0033)	*p195*
indecisive p195	−23±5 (N=88)	90±2 (vs 98±1, p<10^{-5})	−70±11 (vs −54, p=0.27)	22±1 (vs 23, p<0.68)	86%±2 (vs 90%, p<0.12)	255±18 (vs 269, p=0.51)	*p194*
late responder p196	−71±3 (N=59)	82±3 (vs 95, p<10^{-3})	−98±2 (vs −45, p<0.0001)	22±2 (vs 26, p<0.10)	69%±4 (vs 71%, p<0.63)	275±10 (vs 270, p=0.72)	*p190*
biased dp197	−49±5 (N=83)	85±2 (vs 98, p<10^{-6})	−76±9 (vs 66, p<0.0001)	36±1 (vs 31, p<0.011)	87%±4 (vs 86%, p=0.92)	201±6 (vs 189, p=0.22)	n.d.

Mean±SEM values for each assay on 5–6 dpf larvae, significance by t-test (See STAR Methods).